

SEISMIC ATTENUATION SYSTEM SYNTHESIS BY REDUCED ORDER MODELS FROM MULTIBODY ANALYSIS

Valerio Boschi^{†,‡}, Riccardo De Salvo[‡], Pierangelo Masarati^{*}, Giuseppe Quaranta^{*},
Virginio Sannibale[‡]

[†]Università degli studi di Pisa, Dipartimento di Fisica
Largo Bruno Pontecorvo 3, 56127 Pisa, Italy

[‡]California Institute of Technology
1200 East California Blvd, MC 18-34, 91125 Pasadena, CA
e-mail: vboschi@ligo.caltech.edu, desalvo@ligo.caltech.edu,
sannibale_v@ligo.caltech.edu,
web page: <http://www.ligo.caltech.edu/>

^{*}Dipartimento di Ingegneria Aerospaziale, Politecnico di Milano
Via La Masa 34, 20156 Milano, Italy

e-mail: pierangelo.masarati@polimi.it, giuseppe.quaranta@polimi.it,
web page: <http://www.aero.polimi.it/>

Keywords: Structural Dynamics, Computational Mechanics, Vibration Control, Reduced Order Models.

Abstract. *This document describes a method for easily extracting reduced order models from an existing multibody analysis tool, overcoming intrinsic and specific software design limitations. The method addresses the need to automate as much as possible the synthesis of reduced order models from detailed, nonlinear multibody models of complex mechanical systems to support control system design. It is applied to a number of toy models in the context of the free multibody software MBDyn and compared to analytic results. It is also applied to a complex MBDyn model of the Horizontal Access Module Seismic Attenuation System (HAM-SAS) of the Laser Interferometer Gravitational wave Observatory (LIGO) with comparisons to experimental results.*

1 HAM SEISMIC ATTENUATION SYSTEM

The Laser Interferometer Gravitational-Wave Observatory (LIGO) is an experiment, coordinated by the California Institute of Technology and the Massachusetts Institute of Technology (MIT), dedicated to the detection and study of gravitational waves. Technical and scientific research in LIGO is organized through the LIGO Scientific Collaboration (LSC). The experiment consists of three in-vacuum Michelson interferometers with 4 km Fabry-Perot resonant optical cavities. Two interferometers share the same vacuum envelope in Hanford, Washington, and the third is located in Livingston, Louisiana.

Since the performance of ground based gravitational wave detectors is mainly limited by seismic and anthropogenic noise, mechanical isolators are required in order to obtain the design sensitivity.

HAM-SAS (Fig. 1) is a passive seismic attenuation device which is designed to provide 70-80 dB of horizontal and vertical attenuation above 10 Hz [1]. It has been expressly designed to support the optical benches of the Horizontal Access Module (HAM) vacuum chamber of the future Enhanced and Advanced LIGO interferometers.

Two types of tunable mechanical harmonic oscillators are used in the system, namely the inverted pendulum (IP) [2], for attenuation along the horizontal degrees of freedom (DOFs), and the monolithic geometric anti-spring (MGAS) [3], for attenuation along the vertical DOFs. Both devices exploit the property that, at frequencies higher than the oscillator resonance, the transmissibility is equivalent to a second-order low pass filter.

IPs are tunable mechanical oscillators widely used for their good horizontal seismic attenuation performance. Resonant frequencies of tens of millihertz have been reached experimentally in many systems. A counterweight placed below the IP pivot point allows the center of percussion (COP) of the system to be tuned, and substantially improves the attenuation at high frequency.

The MGAS filter (Fig. 2) is a vertical oscillator which uses a crown of curved blades radially compressed in a horizontal plane for the mechanical vertical compliance. The blades are clamped on one end to a plate, and connected on the other end to a small disk. Thanks to this geometry, the load attached to the disk compresses and bends the blades allowing a stable equilibrium position. Acting on the position of the clamps one can change the compression of the blade, and tune the MGAS resonant frequency down to 100 mHz. A device equivalent to the IP counterweight (not shown in the figure) is used to tune the COP to improve the MGAS filter attenuation for frequencies above a few Hz [4].

In the HAM-SAS, four IP legs are arranged in a 1.1 x 0.9 m diamond configuration on a base platform. Four MGAS filters mounted on an intermediate rectangular platform (1.9 x 1.7 m) supported by the IP legs support the optical table. The estimated payload (optical table plus ancillary optics and suspension optics) is approximately 1000 kg.

2 REDUCED ORDER MODELS FROM MULTIBODY ANALYSIS

The design of the control system for the HAM-SAS experiment requires the availability of reduced order models (ROMs) from a structural system that is characterized by significant nonlinearities in a significant number of design points.

The capability of the multibody approach to perform kinematic and dynamic analyses of a complex mechanical system, best suits the modeling needs of this type of problems. This capability is especially desirable in those cases where, as in the MGAS, rigid-body kinematics is mixed with deformable components that are subjected to significant nonlinear effects. Time

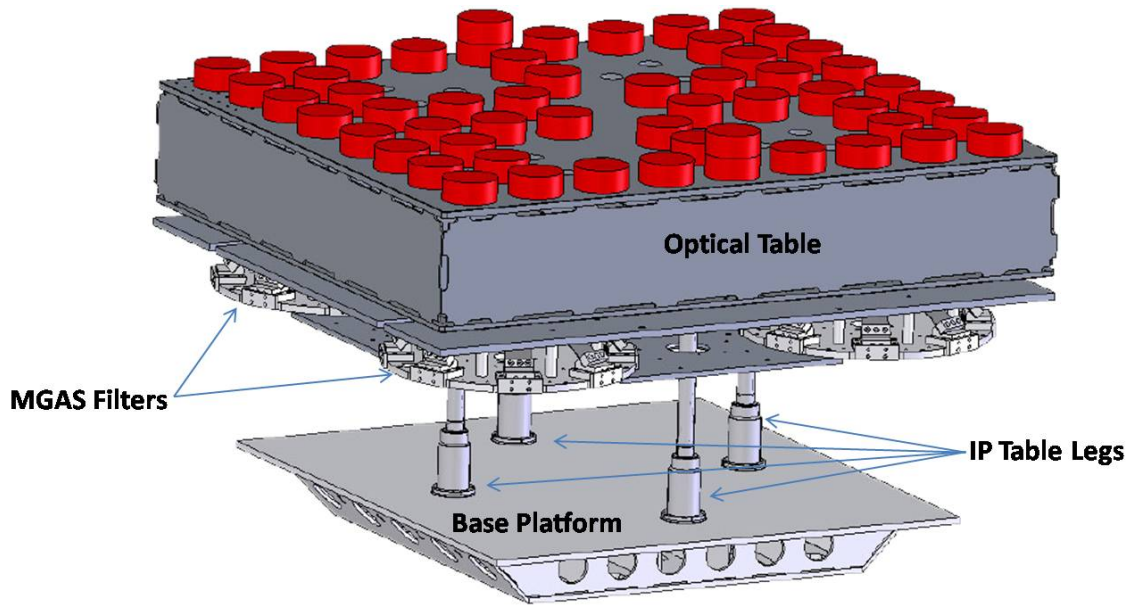


Figure 1: HAM-SAS rendering.

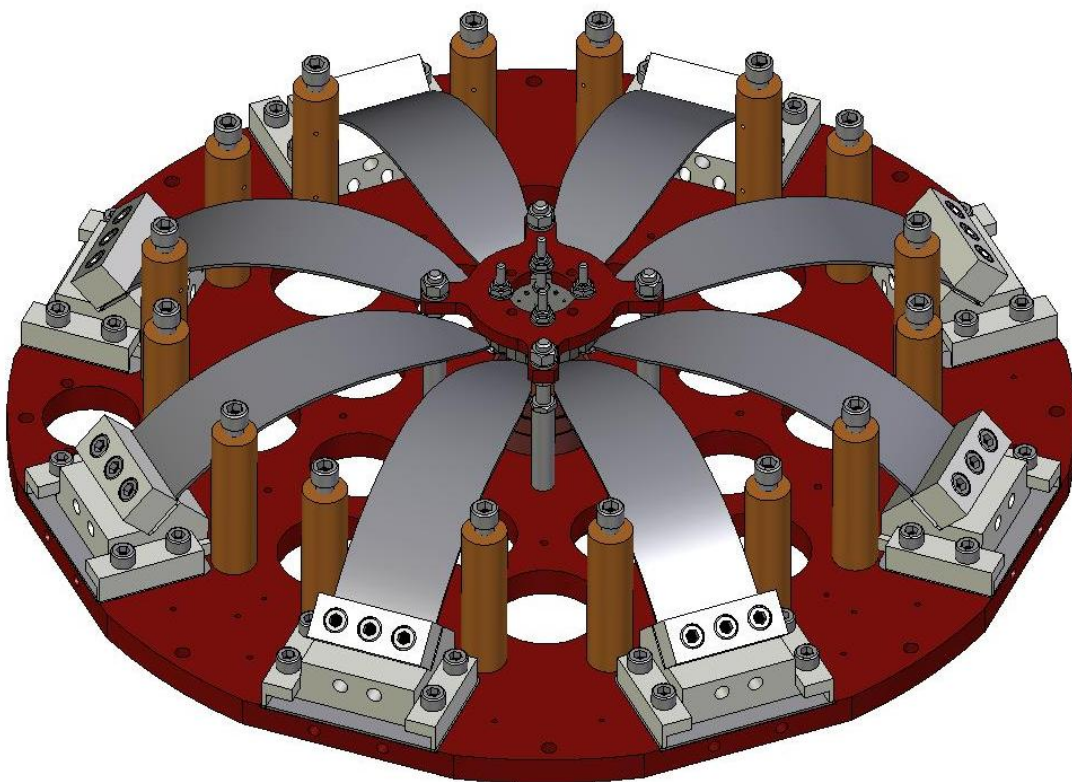


Figure 2: An MGAS filter.

integration of large scale systems, although suitable for problem assessment, may not fit the needs of control system design. In this case, the facility to easily extract reduced order models around arbitrary reference solutions represents a significant advantage because those models can be easily used for control system design.

Normal vibration modes (NVM) are a widely used technique to synthesize ROMs for structural dynamics. However, typical multibody analysis software designed for time integration of generic systems may not allow to easily extract this type of information, because:

- the problem is in the form of a set of differential-algebraic equations (DAE form);
- the problem might not be purely structural;
- system matrices might not be directly available in the appropriate form.

This paper illustrates how normal modes can be extracted directly from an existing, free multibody analysis program (MBDyn, [5]) which, in its current form, suffers from most of the above limitations. It is offered as an alternative to an earlier, successful attempt to extract synthetic information from time-domain analysis focused on an indirect model reduction method based on proper orthogonal decomposition (POD) applied to the transient response [6],

which we mention as a reference and a generic fall-back procedure. that the new approach of this paper works around the existing software limitations and can be implemented with other software and formulations as well.

MBDyn is a free multibody analysis tool [7, 5] that allows one to solve initial value problems (IVPs) directly in the time domain. Typically, a nonlinear DAE in the form

$$\mathbf{F}(\mathbf{y}, \dot{\mathbf{y}}, t) = \mathbf{0}, \quad \mathbf{y}(t_0) = \mathbf{y}_0 \quad (1)$$

is integrated numerically, using a family of implicit multistep integration algorithms, in predictor-corrector form. The predictor determines an estimate of the solution at time step k , based on the solution at earlier time steps. It is typically written in the form

$$\mathbf{y}_k = \sum_{i=1,n} a_i \mathbf{y}_{k-i} + h \sum_{j=0,n} b_j \dot{\mathbf{y}}_{k-j}, \quad (2)$$

where h is the time step [8]. The correction phase uses the perturbed form of Eq. (2),

$$\delta \mathbf{y}_k = h b_0 \delta \dot{\mathbf{y}}_k, \quad (3)$$

to turn the perturbed form of Eq. (1),

$$\mathbf{F} + \mathbf{F}_{/\dot{\mathbf{y}}} \delta \dot{\mathbf{y}} + \mathbf{F}_{/\mathbf{y}} \delta \mathbf{y} = \mathbf{0} \quad (4)$$

into the purely algebraic problem

$$(\mathbf{F}_{/\dot{\mathbf{y}}} + h b_0 \mathbf{F}_{/\mathbf{y}}) \delta \dot{\mathbf{y}} = -\mathbf{F} \quad (5)$$

in $\delta \dot{\mathbf{y}}$ only. The problem being differential-algebraic, both of the matrices appearing in Eq. (5) may be structurally singular. This problem is solved iteratively to convergence for each time step.

The algebraic variables have been included in \mathbf{y} , without any loss in generality; what distinguishes them from the differential ones is the fact that their derivative never directly participates in the problem. However, from another perspective, what participates in the problem should be regarded as the highest order derivative of the variable; this is better illustrated later. Typical mechanical and mechanics-related problems result in DAEs of index 3 [9].

3 MECHANICAL PROBLEM STRUCTURE

When Eq. (1) describes a purely mechanical constrained problem, its formulation in MBDyn schematically resembles

$$\begin{aligned}
M(\mathbf{q}) \dot{\mathbf{q}} - \mathbf{p} &= \mathbf{0} && \text{(momentum definitions)} \\
\dot{\mathbf{p}} - \mathbf{f}(\mathbf{q}, \dot{\mathbf{q}}, t) + \Phi_{/\dot{\mathbf{q}}}^T \boldsymbol{\alpha} &= \mathbf{0} && \text{(equilibrium equations)} \\
\Phi(\mathbf{q}, t) &= \mathbf{0} && \text{(holonomic constraint equations)}
\end{aligned} \tag{6}$$

where only holonomic constraints have been considered for simplicity.

If, without any loss in generality, a linear, constant-coefficient problem is addressed, the structure of Eq. (6) becomes

$$\begin{aligned}
M \dot{\mathbf{q}} - \mathbf{p} &= \mathbf{0} \\
\dot{\mathbf{p}} - \mathbf{f}_{/q} \mathbf{q} - \mathbf{f}_{/\dot{q}} \dot{\mathbf{q}} + \Phi_{/q}^T \boldsymbol{\alpha} &= \mathbf{f} \\
\Phi_{/q} \mathbf{q} &= \mathbf{b}
\end{aligned} \tag{7}$$

where $-\mathbf{f}_{/q}$ and $-\mathbf{f}_{/\dot{q}}$ represent the usual stiffness and damping matrices, respectively. In matrix form, Eq. (7) is

$$\begin{bmatrix} M & \mathbf{0} & \mathbf{0} \\ -\mathbf{f}_{/\dot{q}} & \mathbf{I} & \mathbf{0} \\ \mathbf{0} & \mathbf{0} & \mathbf{0} \end{bmatrix} \begin{Bmatrix} \dot{\mathbf{q}} \\ \dot{\mathbf{p}} \\ \dot{\boldsymbol{\alpha}} \end{Bmatrix} + \begin{bmatrix} \mathbf{0} & -\mathbf{I} & \mathbf{0} \\ -\mathbf{f}_{/q} & \mathbf{0} & \Phi_{/q}^T \\ \Phi_{/q} & \mathbf{0} & \mathbf{0} \end{bmatrix} \begin{Bmatrix} \mathbf{q} \\ \mathbf{p} \\ \boldsymbol{\alpha} \end{Bmatrix} = \begin{Bmatrix} \mathbf{0} \\ \mathbf{f} \\ \mathbf{b} \end{Bmatrix}. \tag{8}$$

However, as detailed later, for purely numerical reasons it may be convenient to consider the algebraic variables $\boldsymbol{\alpha}$ as the time derivatives of a new set of variables $\boldsymbol{\mu}$, so that $\boldsymbol{\alpha} = \dot{\boldsymbol{\mu}}$, and to apply a suitable transformation to the constraint equations that makes their linearization appear as if the derivative of the constraint equation were used. This changes the layout of the matrices in Eq. (8) significantly, yielding

$$\begin{bmatrix} M & \mathbf{0} & \mathbf{0} \\ -\mathbf{f}_{/\dot{q}} & \mathbf{I} & \Phi_{/q}^T \\ \Phi_{/q} & \mathbf{0} & \mathbf{0} \end{bmatrix} \begin{Bmatrix} \dot{\mathbf{q}} \\ \dot{\mathbf{p}} \\ \dot{\boldsymbol{\mu}} \end{Bmatrix} + \begin{bmatrix} \mathbf{0} & -\mathbf{I} & \mathbf{0} \\ -\mathbf{f}_{/q} & \mathbf{0} & \mathbf{0} \\ \mathbf{0} & \mathbf{0} & \mathbf{0} \end{bmatrix} \begin{Bmatrix} \mathbf{q} \\ \mathbf{p} \\ \boldsymbol{\mu} \end{Bmatrix} = \begin{Bmatrix} \mathbf{0} \\ \mathbf{f} \\ \mathbf{b}^* \end{Bmatrix}, \tag{9}$$

where $\mathbf{b}^* = (\partial \mathbf{q} / \partial \dot{\mathbf{q}}) \mathbf{b}$, according to Eq. (3). As a consequence, the amount of manipulation required to exploit the structure of the matrices resulting from mechanical systems changes as well.

In the following, no direct assumption of mechanical problem is made, unless where clearly stated; this description has been given to present some terminology and symbols that will be used throughout this document, and as a reference whenever any mechanical problem assumption is required.

4 REDUCED ORDER MODEL EXTRACTION

Reduced order models may be conveniently used to describe the relevant dynamical behavior of the original system for special purposes, like optimization or control design, that need to be executed rapidly, or repeatedly, or both.

Linear reduced order models may be extracted in different manners: by identifying the relevant dynamics resulting from small perturbations of the system about a steady state solution by

means of some standard identification technique [6], or by linearizing Eq. (1) about the same steady state solution, and by using normal modes and component mode synthesis techniques to extract a reduced model described by a reduced set of degrees of freedom that contain the relevant information about the problem behavior.

In terms of the latter approach, a procedure for the linearization of the model with respect to the state \mathbf{y} and its derivative $\dot{\mathbf{y}}$ can easily be obtained from a program that solves the problem described by Eq. (1), since the linearization is already required in Newton's iteration method of Eq. (5). However, two problems need to be solved to extract useful information from matrices $\mathbf{F}/\dot{\mathbf{y}}$ and \mathbf{F}/\mathbf{y} :

1. the meaning, and the very existence of eigensolutions for a differential-algebraic problem needs to be understood; this problem is common to all formulations, as partially addressed in [6];
2. there could be limitations in the software formulation, that by design it might directly not provide matrices $\mathbf{F}/\dot{\mathbf{y}}$ and \mathbf{F}/\mathbf{y} , so some manipulation could be required to proficiently perform an eigenanalysis; this is the case, for example and in particular, of MBDyn.

5 EIGENANALYSIS

The eigenanalysis problem consists in finding the eigenvalues λ_j and the eigenvectors \mathbf{Y}_j that satisfy

$$(\lambda \mathbf{F}/\dot{\mathbf{y}} + \mathbf{F}/\mathbf{y}) \mathbf{Y} = \mathbf{0}, \quad (10)$$

which may not be a trivial task, as both matrices may be structurally singular. Since the problem is non-symmetric, the eigenanalysis of the adjoint problem

$$(\lambda \mathbf{F}/\dot{\mathbf{y}}^T + \mathbf{F}/\mathbf{y}^T) \mathbf{Y}_{\text{adj}}^T = \mathbf{0}, \quad (11)$$

is required as well, to compute the adjoint eigenvectors \mathbf{Y}_{adj} ; the eigenvalues of the adjoint problem must be the same as the problem in Eq. (10).

Further issues arise when considering how this task needs to be accomplished using MBDyn. In fact, what MBDyn computes, when the `AssJac()` method is invoked to collect the Jacobian matrix of Eq. (5) as required by direct solvers, is

$$\text{AssJac}(\text{dCoef}) = \mathbf{F}/\dot{\mathbf{y}} + \text{dCoef} \cdot \mathbf{F}/\mathbf{y}, \quad (12)$$

where the argument `dCoef` is usually `hb0` as resulting from Eq. (3). Of course, any value of `dCoef` can be passed to the `AssJac()` routine, but exploiting whatever value was used in the matrix already computed for the last good assembly (and factorization, as needed) would save a fair amount of computational time. As a side note, consider that in some cases, MBDyn cannot compute the Jacobian matrix accurately. In this case, it can introduce some simplifications or even ignore the Jacobian. As a consequence, the applicability of the proposed approach is limited to models using only elements whose accurate Jacobian matrix is computed.

In principle, matrices $\mathbf{F}/\dot{\mathbf{y}}$ and \mathbf{F}/\mathbf{y} could be computed by calling `AssJac()` twice: the second time with the opposite of the value used the first time, i.e., `(-dCoef)`. Define

$$\mathbf{J} = \mathbf{F}/\dot{\mathbf{y}} + \text{dCoef} \cdot \mathbf{F}/\mathbf{y} \quad (13)$$

$$\mathbf{J}^* = \mathbf{F}/\dot{\mathbf{y}} - \text{dCoef} \cdot \mathbf{F}/\mathbf{y}; \quad (14)$$

then

$$\mathbf{F}/\mathbf{y} = \frac{\mathbf{J} + \mathbf{J}^*}{2} \quad (15)$$

$$\mathbf{F}/\mathbf{y} = \frac{\mathbf{J} - \mathbf{J}^*}{2 \cdot \text{dCoeF}}. \quad (16)$$

The eigenproblem of Eq. (10) becomes

$$\left(\lambda \frac{\mathbf{J} + \mathbf{J}^*}{2} + \frac{\mathbf{J} - \mathbf{J}^*}{2 \cdot \text{dCoeF}} \right) \mathbf{Y} = \mathbf{0} \quad (17)$$

To limit the amount of required matrix manipulation, each matrix in Eq. (17) can be conveniently collected, yielding

$$(\Lambda \mathbf{J} + \mathbf{J}^*) \mathbf{Y} = \mathbf{0}, \quad (18)$$

where

$$\Lambda = \frac{\lambda \cdot \text{dCoeF} + 1}{\lambda \cdot \text{dCoeF} - 1}, \quad (19)$$

which recalls the reverse of the Tustin transformation from continuous to discrete time (dCoeF is hb_0 , and $b_0 = 1/2$ when the Crank-Nicholson integration scheme is used). This implies that the presence of dCoeF in the matrices somehow biases the resulting eigenvalues. In fact, valid λ must be $0 \leq |\lambda| < 1/\text{dCoeF}$, and the closer they get to the upper bound, the less accurate they are, so $1/\text{dCoeF}$ represents sort of a Nyquist frequency.

Notice that if at least one iteration was required for converging at the time step where eigenvalue extraction is requested, matrix \mathbf{J} has already been factored. Thus, the eigenproblem of Eq. (18) could be rewritten as

$$\Lambda \mathbf{Y} = -(\mathbf{J}^{-1} \mathbf{J}^*) \mathbf{Y}, \quad (20)$$

if necessary. This operation is not recommended because it destroys the sparsity of the matrices \mathbf{J} and \mathbf{J}^* . However, efficient methods to extract a reduced set of eigenvalues and eigenvectors, like those based on subspace iteration and similar, could take advantage of this form without actually computing matrix $\mathbf{J}^{-1} \mathbf{J}^*$, but rather performing sequences of matrix-vector multiplications and back-substitutions, namely

$$\mathbf{J}^{-1} \mathbf{J}^* \mathbf{Y} = \mathbf{J}^{-1} \hat{\mathbf{Y}}, \quad (21)$$

with

$$\hat{\mathbf{Y}} = \mathbf{J}^* \mathbf{Y}. \quad (22)$$

Typically, model reduction of mechanical systems requires one to consider complex-conjugate eigenvalues λ that are close to purely imaginary, in a range that goes from zero to an upper bound. Eigenvalue extraction techniques that allow one to efficiently collect the desired subset of eigenvalues usually require one to center the desired range in a certain point of the complex plane, by means of some eigenvalue shift technique. In the case of Eq. (19), $\lambda = 0$ corresponds to $\Lambda = -1$.

The actual eigenvalues can be computed from Eq. (19) as

$$\lambda = \frac{1}{\text{dCoeF}} \frac{\Lambda + 1}{\Lambda - 1} \quad (23)$$

This problem, for a system with n structural nodes and m algebraic constraints, basically gives three types of eigenvalues:

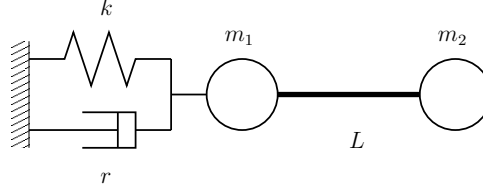


Figure 3: Two masses problem.

- a) the usual ones, related to the dynamics of the system ($12n - 2m$);
- b) those related to the constrained kinematic variables ($2m$), which have no dynamics and thus should yield infinite eigenvalues (this may no longer be true because of some special arranging of equations and variables, as discussed later);
- c) those related to the Lagrange multipliers (m), which give infinite eigenvalues as well.

The eigenvectors of the modified problem of Eq. (18) are the same as those of the original one.

6 NUMERICAL EXAMPLES

In order to clarify the above description, a few examples of increasing complexity are analyzed, and numerical results are extracted either analytically, resembling the procedure that would be used by MBDyn, or directly from the multibody software. These are compared to analytical solutions when available.

6.1 Two Rigidly Connected Masses

Consider the system of two masses illustrated in Fig. 3; the first mass is connected to the ground by a spring and a damper, while the motion of the second mass is constrained to track that of the first one by a holonomic algebraic constraint:

$$m_1 \dot{x}_1 - q_1 = 0 \quad (\text{mass 1 momentum definition}) \quad (24)$$

$$\dot{q}_1 + r \dot{x}_1 + kx_1 - \alpha = 0 \quad (\text{mass 1 equilibrium}) \quad (25)$$

$$m_2 \dot{x}_2 - q_2 = 0 \quad (\text{mass 2 momentum definition}) \quad (26)$$

$$\dot{q}_2 + \alpha = f \quad (\text{mass 2 equilibrium}) \quad (27)$$

$$x_2 - x_1 = L \quad (\text{holonomic constraint}) \quad (28)$$

In matrix notation:

$$\begin{bmatrix} m_1 & 0 & 0 & 0 & 0 \\ r & 1 & 0 & 0 & 0 \\ 0 & 0 & m_2 & 0 & 0 \\ 0 & 0 & 0 & 1 & 0 \\ 0 & 0 & 0 & 0 & 0 \end{bmatrix} \begin{Bmatrix} \dot{x}_1 \\ \dot{q}_1 \\ \dot{x}_2 \\ \dot{q}_2 \\ \dot{\alpha} \end{Bmatrix} + \begin{bmatrix} 0 & -1 & 0 & 0 & 0 \\ k & 0 & 0 & 0 & -1 \\ 0 & 0 & 0 & -1 & 0 \\ 0 & 0 & 0 & 0 & 1 \\ -1 & 0 & 1 & 0 & 0 \end{bmatrix} \begin{Bmatrix} x_1 \\ q_1 \\ x_2 \\ q_2 \\ \alpha \end{Bmatrix} = \begin{Bmatrix} 0 \\ 0 \\ 0 \\ f \\ L \end{Bmatrix} \quad (29)$$

Note that matrix $\mathbf{F}_{/\dot{\mathbf{y}}}$ is singular, while matrix $\mathbf{F}_{/\mathbf{y}}$ is not because of the spring.

In systems of DAEs whose index is larger than 1, the algebraic variables do not directly participate in the algebraic portion of the system. As a consequence, the linearization of algebraic constraints results in equations where all coefficients multiply differential variables, and thus are multiplied by $\text{dCoe}f$. This may result in bad matrix scaling, so it may be convenient to

Table 1: Two mass example data

Parameter	Value
m_1	2.0 kg
m_2	8.0 kg
k	1000.0 N/m
r	10.0 Ns/m

Table 2: Two mass example results: eigenvalues in the undamped case (radian/s)

	Exact	Eq. (29)	Eq. (30)
spring/mass	$+j \cdot 10.0$	$+j \cdot 10.0$	$+j \cdot 10.0$
spring/mass	$-j \cdot 10.0$	$-j \cdot 10.0$	$-j \cdot 10.0$
constrained variables	—	∞	0.0
constrained variables	—	∞	0.0
Lagrange multiplier	—	∞	∞

divide those equations by `dCoeF` to improve the factorization and thus the convergence of the iteration [9].

As stated earlier, the multiplier α , which represents the algebraic portion of the variables, should be considered the derivative of a new variable, μ , so that its contribution to the Jacobian matrix of the problem moves to matrix $\mathbf{F}/\dot{\mathbf{y}}$. Furthermore, the algebraic Equation (28) can be conveniently divided by `dCoeF`. The modified problem becomes

$$\begin{bmatrix} m_1 & 0 & 0 & 0 & 0 \\ r & 1 & 0 & 0 & -1 \\ 0 & 0 & m_2 & 0 & 0 \\ 0 & 0 & 0 & 1 & 1 \\ -1 & 0 & 1 & 0 & 0 \end{bmatrix} \begin{Bmatrix} \dot{x}_1 \\ \dot{q}_1 \\ \dot{x}_2 \\ \dot{q}_2 \\ \dot{\mu} \end{Bmatrix} + \begin{bmatrix} 0 & -1 & 0 & 0 & 0 \\ k & 0 & 0 & 0 & 0 \\ 0 & 0 & 0 & -1 & 0 \\ 0 & 0 & 0 & 0 & 0 \\ 0 & 0 & 0 & 0 & 0 \end{bmatrix} \begin{Bmatrix} x_1 \\ q_1 \\ x_2 \\ q_2 \\ \mu \end{Bmatrix} = \begin{Bmatrix} 0 \\ 0 \\ 0 \\ f \\ L/\text{dCoeF} \end{Bmatrix} \quad (30)$$

The above problem is equivalent to a single spring/mass/damper system whose spring and damping values are k and r respectively and whose mass is $m_1 + m_2$; so, when no damping is present, its two eigenvalues are $\lambda_{1|2} = \pm j \cdot \sqrt{k/(m_1 + m_2)}$.

By way of a numerical example, consider the data in Table 1; for $r = 0$ the exact solution is ± 10.0 radian/s for the two valid modes. Both the representations of Eqs. (29, 30) yield the exact value regardless of the value of `dCoeF` (it has been set to 0.001 for the presented results), as indicated in Table 2. However, while using the form of Eq. (29) results in an infinite value for all the remaining eigenvalues, using that of Eq. (30) results in an infinite value only for the eigenvalue that refers to the Lagrange multiplier, while the eigenvalues related to the constrained variables are zero.

The same occurs when r assumes the value given in Table 1: both formulations yield the same eigenvalues,

$$\lambda_{1|2} = -0.5 \pm j \cdot 9.9875 \text{ radian/s} \quad (31)$$

and the same considerations discussed in Table 2 apply to the remaining eigenvalues.

Being able to estimate which eigenvalues are actually zero because of referring to constrained variables is often important because it is desirable to eliminate the corresponding eigenvectors from the reduced basis. In the presence of numerical errors in the eigenvalue extraction, any of the Λ resulting from the eigensolution may be affected by an error ε ; as a consequence,

according to Eq. (23), the corresponding continuous time eigenvalues would be

$$\lambda = \frac{1}{\text{dCoef}} \frac{\Lambda + \varepsilon + 1}{\Lambda + \varepsilon - 1}. \quad (32)$$

The sensitivity of the eigenvalues to the error is

$$\frac{\partial \lambda}{\partial \varepsilon} = \frac{1}{\text{dCoef}} \left(\frac{1}{\Lambda + \varepsilon - 1} - \frac{\Lambda + \varepsilon - 1}{(\Lambda + \varepsilon + 1) 2} \right). \quad (33)$$

Their value, when $\Lambda \rightarrow -1$, corresponding to a zero-valued eigenvalue, is

$$\lim_{\Lambda \rightarrow -1} \lambda = \frac{1}{\text{dCoef}} \frac{\varepsilon}{\varepsilon - 2} \quad (34)$$

$$\lim_{\Lambda \rightarrow -1} \frac{\partial \lambda}{\partial \varepsilon} = \frac{1}{\text{dCoef}} \frac{-2}{(\varepsilon - 2) 2}. \quad (35)$$

The availability of an estimate of the quality of the computed eigenvalues allows one to set a threshold for which eigenvectors must be discarded.

6.2 Buckling of a Simply-Supported Beam

The buckling of a simply-supported, straight, uniform beam, illustrated in Fig. 4, is analyzed by performing an eigensolution of the matrices extracted from the multibody solver.

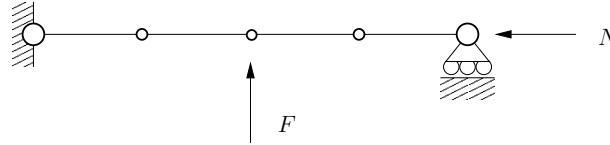


Figure 4: Simply-supported, straight uniform beam model.

Since the multibody solver is not designed to directly perform eigensolutions, a model consisting of a simply supported beam, implemented with the Finite Volume scheme proposed in [10] and with lumped inertia, is analyzed at different axial compression load levels, corresponding to specified fractions of the nominal critical load

$$N_{\text{critical}} = \left(\frac{\pi}{L} \right) 2EJ, \quad (36)$$

as a function of the bending stiffness EJ and the beam length L . The resulting angular frequencies are shown in Fig. 5, compared to the analytical values

$$\omega = \sqrt{\frac{\left(\frac{\pi}{L} \right) 4EJ - \left(\frac{\pi}{L} \right) 2N}{\rho A}} = \left(\frac{\pi}{L} \right) 2 \sqrt{\frac{EJ}{\rho A}} \sqrt{1 - \frac{N}{N_{\text{critical}}}}, \quad (37)$$

where ρA is the mass per unit length of the beam. The error is below 1.6% with 2 beam elements, and drops to 0.8% with 4. The mode shape corresponding to the first bending mode, without axial compression load, is shown in Fig. 6. The analysis of the free response of the beam by means of the POD formulation presented in [6] yields exactly the same result for both the frequency and the mode shape.

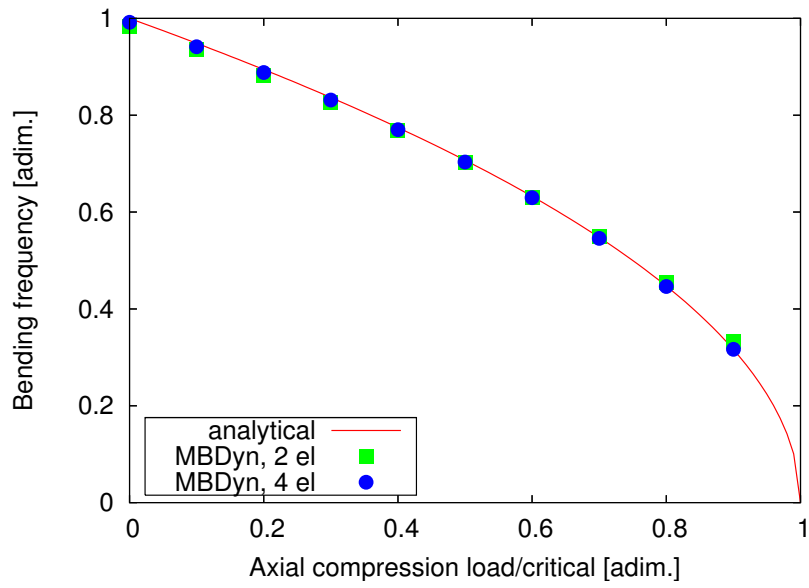


Figure 5: First bending mode angular frequency as function of the axial compression load.

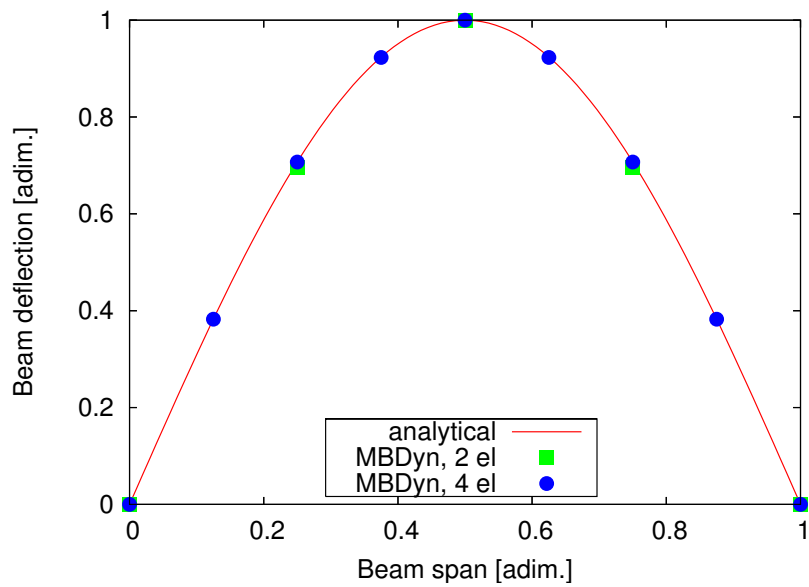


Figure 6: First bending mode shape without axial compression load.

7 STATE-SPACE MODEL

A state-space (SS) model is obtained from the eigenanalysis by projecting the matrices $\mathbf{F}_{/y}$, $\mathbf{F}_{/y}$ onto the space of the eigenvectors \mathbf{Y} , \mathbf{Y}_{adj} ; typically, a subset of the eigenvalues and eigenvectors of the original system are selected, which fulfill appropriate requirements in terms of quality of the description of the original dynamics and of coverage of the expected input spectrum.

Input and output selection is done by defining matrices $\tilde{\mathbf{B}}$ and $\tilde{\mathbf{C}}$ that map the space of inputs \mathbf{u} on that of the force perturbations $-\Delta\mathbf{F}$, and the space of the variables $\Delta\mathbf{y}$ on that of the outputs \mathbf{z} :

$$-\Delta\mathbf{F} = \tilde{\mathbf{B}}\mathbf{u} \quad (38)$$

$$\mathbf{z} = \tilde{\mathbf{C}}\Delta\mathbf{y} \quad (39)$$

Starting from

$$\mathbf{F}_{/y}\Delta\dot{\mathbf{y}} + \mathbf{F}_{/y}\Delta\mathbf{y} = -\Delta\mathbf{F}, \quad (40)$$

where Eq. (38) needs to be substituted, and from Eq. (39), the variable substitution

$$\Delta\mathbf{y} = \tilde{\mathbf{Y}}\mathbf{x} \quad (41)$$

is applied, where $\tilde{\mathbf{Y}}$ represents the desired selection of eigenvectors. In general, the eigenvectors resulting from the eigenanalysis will be either real or complex-conjugate, depending on the eigenvalue they relate to, since they result from real matrices. In order to keep the matrices real, it is convenient to combine complex-conjugate pairs of eigenvectors by means of a matrix

$$\mathbf{T} = \frac{1}{2} \begin{bmatrix} 1 & -j \\ 1 & j \end{bmatrix}, \quad (42)$$

so that they are split into their real and imaginary parts.

Eq. (40) is then projected onto the space of the corresponding adjoint eigenvectors $\tilde{\mathbf{Y}}_{\text{adj}}$:

$$\tilde{\mathbf{Y}}_{\text{adj}}\mathbf{F}_{/y}\tilde{\mathbf{Y}}\dot{\mathbf{x}} + \tilde{\mathbf{Y}}_{\text{adj}}\mathbf{F}_{/y}\tilde{\mathbf{Y}}\mathbf{x} = \tilde{\mathbf{Y}}_{\text{adj}}\tilde{\mathbf{B}}\mathbf{u}, \quad (43)$$

while Eq. (39) becomes

$$\mathbf{z} = \tilde{\mathbf{C}}\tilde{\mathbf{Y}}\mathbf{x}. \quad (44)$$

The whole set of equations is cast into a descriptor state-space representation

$$\mathbf{E}\dot{\mathbf{x}} = \mathbf{A}\mathbf{x} + \mathbf{B}\mathbf{u} \quad (45)$$

$$\mathbf{z} = \mathbf{C}\mathbf{x} \quad (46)$$

by defining

$$\mathbf{E} = \tilde{\mathbf{Y}}_{\text{adj}}\mathbf{F}_{/y}\tilde{\mathbf{Y}} \quad (47)$$

$$\mathbf{A} = -\tilde{\mathbf{Y}}_{\text{adj}}\mathbf{F}_{/y}\tilde{\mathbf{Y}} \quad (48)$$

$$\mathbf{B} = \tilde{\mathbf{Y}}_{\text{adj}}\tilde{\mathbf{B}} \quad (49)$$

$$\mathbf{C} = \tilde{\mathbf{C}}\tilde{\mathbf{Y}}, \quad (50)$$

with \mathbf{E} and \mathbf{A} square and possibly singular, but with $\mathbf{A} - \lambda\mathbf{E}$ representing a regular matrix pencil.

The physical meaning of the descriptor form is that some choice of the reduced coordinates might lead to a differential-algebraic problem, indicating that some of the coordinates actually describe an essentially static behavior of the system. An appropriate decomposition, e.g. the singular value decomposition (SVD), applied to matrix \mathbf{E} , leads to computing a set of matrices

$$\mathbf{U}\mathbf{\Sigma}\mathbf{V}^T = \mathbf{E}, \quad (51)$$

with \mathbf{U} and \mathbf{V} full rank orthogonal, and $\mathbf{\Sigma}$ diagonal positive definite, or semi-definite in the case that \mathbf{E} is not full rank. These allow the problem to be rewritten in the form

$$\mathbf{\Sigma}\dot{\boldsymbol{\xi}} = \mathbf{U}^T \mathbf{A} \mathbf{V} \boldsymbol{\xi} + \mathbf{U}^T \mathbf{B} \mathbf{u} \quad (52)$$

$$\mathbf{z} = \mathbf{C} \mathbf{V} \boldsymbol{\xi} \quad (53)$$

in the new coordinates $\boldsymbol{\xi}$, which can be partitioned into a dynamic subset $\boldsymbol{\xi}_d$, related to the non-zero diagonal coefficients of $\mathbf{\Sigma}$, and a static subset $\boldsymbol{\xi}_s$, related to the remaining zero diagonal coefficients. The problem becomes

$$\mathbf{\Sigma}_d \dot{\boldsymbol{\xi}}_d = \mathbf{U}_d^T \mathbf{A} \mathbf{V}_d \boldsymbol{\xi}_d + \mathbf{U}_d^T \mathbf{A} \mathbf{V}_s \boldsymbol{\xi}_s + \mathbf{U}_d^T \mathbf{B} \mathbf{u} \quad (54)$$

$$\mathbf{0} = \mathbf{U}_s^T \mathbf{A} \mathbf{V}_d \boldsymbol{\xi}_d + \mathbf{U}_s^T \mathbf{A} \mathbf{V}_s \boldsymbol{\xi}_s + \mathbf{U}_s^T \mathbf{B} \mathbf{u} \quad (55)$$

$$\mathbf{z} = \mathbf{C} \mathbf{V}_d \boldsymbol{\xi}_d + \mathbf{C} \mathbf{V}_s \boldsymbol{\xi}_s. \quad (56)$$

But Eq. (55) is static; so it can be solved for $\boldsymbol{\xi}_s$ as

$$\boldsymbol{\xi}_s = -(\mathbf{U}_s^T \mathbf{A} \mathbf{V}_s)^{-1} (\mathbf{U}_s^T \mathbf{A} \mathbf{V}_d \boldsymbol{\xi}_d + \mathbf{U}_s^T \mathbf{B} \mathbf{u}), \quad (57)$$

since matrix $\mathbf{U}_s^T \mathbf{A} \mathbf{V}_s$ must be non-singular when \mathbf{E} and \mathbf{A} represent a regular matrix pencil.

When $\boldsymbol{\xi}_s$ is substituted in Eqs. (54, 56), the problem becomes

$$\dot{\boldsymbol{\xi}}_d = \bar{\mathbf{A}} \boldsymbol{\xi}_d + \bar{\mathbf{B}} \mathbf{u} \quad (58)$$

$$\mathbf{z} = \bar{\mathbf{C}} \boldsymbol{\xi}_d + \bar{\mathbf{D}} \mathbf{u}, \quad (59)$$

with

$$\bar{\mathbf{A}} = \mathbf{\Sigma}_d^{-1} \mathbf{U}_d^T \left(\mathbf{I} - \mathbf{A} \mathbf{V}_s (\mathbf{U}_s^T \mathbf{A} \mathbf{V}_s)^{-1} \mathbf{U}_s^T \right) \mathbf{A} \mathbf{V}_d \quad (60)$$

$$\bar{\mathbf{B}} = \mathbf{\Sigma}_d^{-1} \mathbf{U}_d^T \left(\mathbf{I} - \mathbf{A} \mathbf{V}_s (\mathbf{U}_s^T \mathbf{A} \mathbf{V}_s)^{-1} \mathbf{U}_s^T \right) \mathbf{B} \quad (61)$$

$$\bar{\mathbf{C}} = \mathbf{C} \left(\mathbf{I} - \mathbf{V}_s (\mathbf{U}_s^T \mathbf{A} \mathbf{V}_s)^{-1} \mathbf{U}_s^T \mathbf{A} \right) \mathbf{V}_d \quad (62)$$

$$\bar{\mathbf{D}} = -\mathbf{C} \mathbf{V}_s (\mathbf{U}_s^T \mathbf{A} \mathbf{V}_s)^{-1} \mathbf{U}_s^T \mathbf{B}, \quad (63)$$

thus introducing a direct transmission term into an ordinary state-space representation of the dynamic part of the reduced model.

Due to the previously described way MBDyn computes matrices $\mathbf{F}_{/y}$ and $\mathbf{F}_{/y}$, the reduction procedure must actually be implemented as

$$\mathbf{E} = \tilde{\mathbf{Y}}_{\text{adj.}} \frac{\mathbf{J} + \mathbf{J}^*}{2} \tilde{\mathbf{Y}} \quad (64)$$

$$\mathbf{A} = -\tilde{\mathbf{Y}}_{\text{adj.}} \frac{\mathbf{J} - \mathbf{J}^*}{2 \text{dCoeF}} \tilde{\mathbf{Y}}, \quad (65)$$

Table 3: Simply-supported beam properties

Parameter	Value	
L	1.0	m
EA	1.0e+6	N
GA	1.0e+6	N
GJ	1.0e+3	Nm ²
EJ	1.0e+3	Nm ²
ρA	1.0	kg/m

where matrices \mathbf{E} and \mathbf{A} from Eqs. (47, 48) are computed by means of Eqs. (15, 16). The above expressions may be conveniently expanded into

$$\mathbf{E} = \frac{1}{2} \left(\tilde{\mathbf{Y}}_{\text{adj.}} \mathbf{J} \tilde{\mathbf{Y}} + \tilde{\mathbf{Y}}_{\text{adj.}} \mathbf{J}^* \tilde{\mathbf{Y}} \right) \quad (66)$$

$$\mathbf{A} = -\frac{1}{2 \text{dCoef}} \left(\tilde{\mathbf{Y}}_{\text{adj.}} \mathbf{J} \tilde{\mathbf{Y}} - \tilde{\mathbf{Y}}_{\text{adj.}} \mathbf{J}^* \tilde{\mathbf{Y}} \right) \quad (67)$$

when a significant order reduction occurs because a limited number of generalized coordinates has been selected.

7.1 Application to the Simply-Supported Beam

Consider the previously described 4-beam element model of a simply-supported beam, without any axial compression load. The properties of the beam are given in Table 3.

When only the first bending mode is considered, the above approach yields a model described by matrices

$$\mathbf{E} = \begin{bmatrix} 6.5212\text{e-}15 & 3.4772\text{e-}13 \\ 2.8804\text{e-}12 & -5.4033\text{e-}14 \end{bmatrix} \quad (68)$$

$$\mathbf{A} = \begin{bmatrix} -1.0765\text{e-}10 & 2.0193\text{e-}12 \\ 1.6728\text{e-}11 & 8.9170\text{e-}10 \end{bmatrix}, \quad (69)$$

whose eigenvalues are exactly those of the first beam bending mode, $\lambda_{1|2} = \pm j309.58$ radian/s.

When considering the mid-span node as input and output, the model is completed by matrices

$$\mathbf{B} = \begin{bmatrix} -1.3271\text{e-}10 \\ 6.3297\text{e-}03 \end{bmatrix} \quad (70)$$

$$\mathbf{C} = \begin{bmatrix} -5.4828\text{e-}14 & -2.9227\text{e-}12 \end{bmatrix}. \quad (71)$$

The static response of the reduced order model, provided \mathbf{A} is not singular, is obtained by setting $\dot{\mathbf{x}}$ to zero in Eq. (45), then solving Eq. (45) with respect to \mathbf{x} and substituting it into Eq. (46), namely

$$\mathbf{z}_{\text{static}} = -\mathbf{C} \mathbf{A}^{-1} \mathbf{B} \mathbf{u}. \quad (72)$$

The reduced order model yields the static response within less than 1.6% of the corresponding response of the multibody analysis, which in turn exactly captures the static solution, including the shear effect

$$z_{\text{mid-span}} = \left(\frac{L3}{48 EJ} + \frac{L}{4 GA} \right) f_{\text{mid-span}}, \quad (73)$$

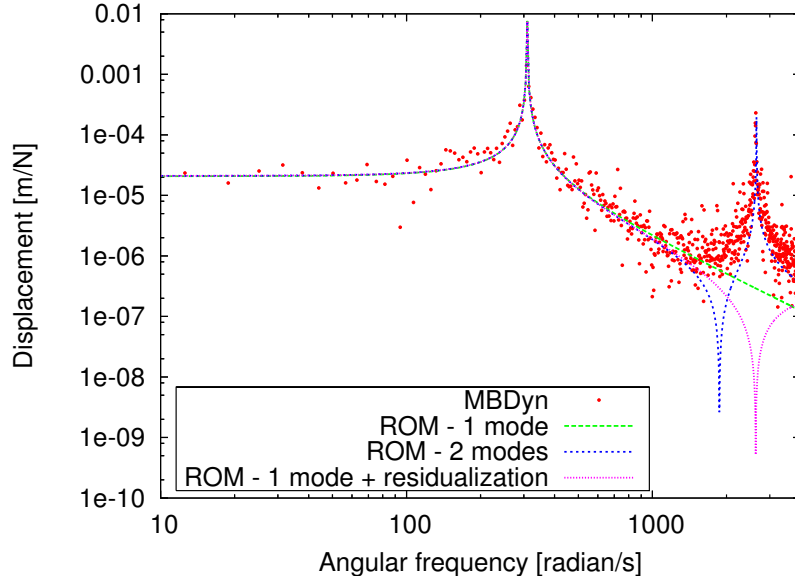


Figure 7: Dynamic response of the mid-span point of the simply-supported beam, modeled with 4 elements, to a co-located force excitation, compared to the single- and two-mode ROMs, the latter also with statical residualization of the higher frequency mode.

as shown in [10].

When adding a second mode, namely the third bending mode of the simply-supported beam, since all even modes show a nodal point at mid-span, the reduced-order model matrices become

$$\mathbf{E} = \begin{bmatrix} -2.5973e-12 & 2.0793e-10 & 1.5948e-16 & 8.5811e-15 \\ 1.9366e-09 & 2.4191e-11 & -4.3476e-21 & 9.9766e-25 \\ -1.8330e-13 & 1.4675e-11 & 6.5212e-15 & 3.4772e-13 \\ -2.2645e-20 & 1.4809e-19 & 2.8804e-12 & -5.4033e-14 \end{bmatrix} \quad (74)$$

$$\mathbf{A} = \begin{bmatrix} -5.5062e-07 & -6.8777e-09 & -2.6565e-12 & 4.9835e-14 \\ -6.4057e-08 & 5.1283e-06 & -2.0536e-21 & 2.6097e-20 \\ -3.8859e-08 & -4.8539e-10 & -1.0765e-10 & 2.0193e-12 \\ -4.0203e-16 & -1.1683e-16 & 1.6728e-11 & 8.9170e-10 \end{bmatrix}, \quad (75)$$

yielding the additional eigenvalues $\lambda_{3|4} = \pm j2648.03$ radian/s, which represent a poor estimate of the third bending frequency since a 4-beam element model is too coarse, and

$$\mathbf{B} = \begin{bmatrix} 1.6122e-15 \\ 1.4495e-03 \\ -1.3271e-10 \\ 6.3297e-03 \end{bmatrix} \quad (76)$$

$$\mathbf{C} = [1.2893e-11 \quad -1.0322e-09 \quad -5.4828e-14 \quad -2.9227e-12]. \quad (77)$$

This model yields the static response within 0.2%.

The dynamic response of both the previously discussed ROMs is illustrated in Fig. 7, compared to the frequency content of the direct response of the multibody analysis when excited by a low-pass filtered random input. The figure also shows the response of the two-mode ROM

Table 4: Pendulum example data

Parameter	Value	
m	1.0	kg
J	0.001	kg m ²
L	1.0	m
g	9.81	m/s ²

when the higher-frequency mode is statically residualized. The corresponding matrices are

$$\overline{\mathbf{A}} = \begin{bmatrix} 1.3140\text{e-}08 & 3.0958\text{e+}02 \\ -3.0958\text{e+}02 & 1.3151\text{e-}03 \end{bmatrix} \quad (78)$$

$$\overline{\mathbf{B}} = \begin{bmatrix} 2.1972\text{e+}09 \\ 9.4722\text{e+}03 \end{bmatrix} \quad (79)$$

$$\overline{\mathbf{C}} = [1.8182\text{e-}19 \quad -2.9232\text{e-}12] \quad (80)$$

$$\overline{\mathbf{D}} = [2.9177\text{e-}07] . \quad (81)$$

As expected, they yield exactly the same eigenvalues of the single-mode ROM, which also correspond to the low-frequency eigenvalues of the two-mode ROM, along with the same static response of the two-mode ROM.

7.2 Simple Pendulum

Consider now the deceptively simple example of a simple pendulum, where the effect corresponding to the stiffness originates from the kinematics of the system and the presence of mass and a uniform force field.

The properties of the model are illustrated in Table 4. The model consists of a rigid body, connected to the ground node by a revolute hinge, and immersed in a uniform force field. It amounts to 29 equations (6 for the ground node, 12 for the pendulum node, 6 to clamp the ground node and 5 for the revolute hinge), but its dynamics are actually described by a second-order system, whose eigenvalues are

$$\lambda_{1|2} = \pm j \sqrt{\frac{g/L}{1 + \frac{J}{mL^2}}} . \quad (82)$$

For the problem at hand, they result in $\lambda_{1|2} = \pm j3.1305$ radian/s.

The corresponding reduced model obtained with the proposed procedure is described by matrices

$$\mathbf{E} = \begin{bmatrix} -9.8852\text{e-}18 & 1.6266\text{e-}04 \\ 1.6266\text{e-}01 & 1.1370\text{e-}14 \end{bmatrix} \quad (83)$$

$$\mathbf{A} = \begin{bmatrix} 5.0921\text{e-}04 & 5.4210\text{e-}17 \\ 2.7756\text{e-}14 & -5.0921\text{e-}01 \end{bmatrix} \quad (84)$$

$$\mathbf{B} = \begin{bmatrix} 0.0000\text{e+}00 \\ 2.9087\text{e-}01 \end{bmatrix} \quad (85)$$

$$\mathbf{C} = [-5.5866\text{e-}04 \quad 1.7846\text{e-}01] , \quad (86)$$

which give the pendulum angle as function of an input torque. They yield the static response and the eigenvalues of the problem exactly. The eigenvectors of the original system, related to the eigenvalues that describe the dynamics of the pendulum, correctly show that the ratio between the displacement and the rotation of the pendulum node is exactly L .

Consider now the previous problem when the pendulum is inverted, that is, in the unstable equilibrium condition. In that case, the eigenvalues of the problem are

$$\lambda_{1|2} = \pm \sqrt{\frac{g/L}{1 + \frac{J}{mL^2}}}, \quad (87)$$

which are real and distinct, and one of them is unstable; for the problem at hand, they are $\lambda_{1|2} = \pm 3.1305$ radian/s. The corresponding reduced model obtained with the proposed procedure is

$$\mathbf{E} = \begin{bmatrix} -1.6282e-01 & -1.6250e-01 \\ -1.6250e-01 & -1.6282e-01 \end{bmatrix} \quad (88)$$

$$\mathbf{A} = \begin{bmatrix} 5.0972e-01 & -5.0870e-01 \\ 5.0870e-01 & -5.0972e-01 \end{bmatrix} \quad (89)$$

$$\mathbf{B} = \begin{bmatrix} 2.9087e+01 \\ 2.9087e-01 \end{bmatrix} \quad (90)$$

$$\mathbf{C} = [1.7846e-04 \quad -1.7846e-01]; \quad (91)$$

they reproduce exactly the eigenvalues of the problem.

This illustrates that the proposed procedure can also be used to extract reduced order models from unstable systems, which may be required to design a control that stabilizes the system. In this case the procedure may be critical in that obtaining a static equilibrium solution from an unstable system may be an issue.

8 APPLICATION TO HAM-SAS

8.1 HAM-SAS MBDyn Modeling

Although the most common way to simulate a complex mechanical system is by means of Finite-Element Modeling (FEM) techniques, this approach for HAM-SAS was not entirely successful. Even though FEM simulations have been useful to study the internal modes of the rigid structure, they were unable to accurately reproduce the dynamic behavior, especially at low frequency.

For this reason, a multibody approach was preferred. As shown in the sketch of Fig. 8, the MBDyn model of the HAM-SAS mechanical structure incorporates

- **11 Rigid Bodies:** 1 massive *Base* used to excite the system with respect to the ground in all six DOFs through a force/position actuator, 1 *Optical Table*, 1 *Spring Box*, 4 *Inverted Pendulum* (IP) legs, 4 *Little Pendulums*;
- **4 Angular Springs** with 3D diagonal stiffness and viscous matrices representing the flexible joints at the bottom of the IP legs;
- **4 Linear Springs** with 3D diagonal stiffness matrix representing the MGAS springs;

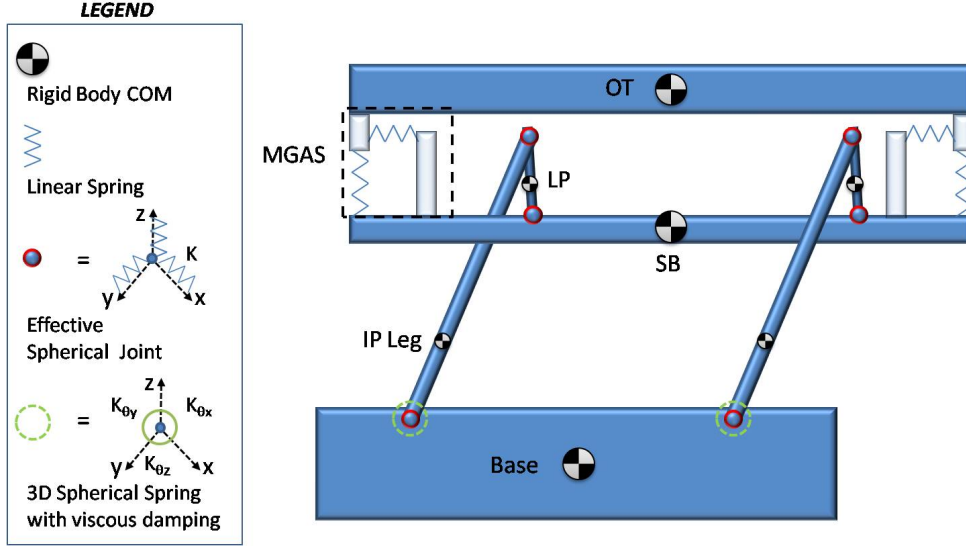


Figure 8: Sketch of a y - z section of the HAM-SAS mechanical model developed with MBDyn.

- **12 Spherical Joints:** 8 connecting the *Little Pendulums* to the *Spring Box* and to the *Optical Table*, 4 connecting the *IP legs* to the *Base*;
- **8 Displacement Sensors** placed on the *Spring Box* that measure its position with respect to the *Base*;
- **8 Force Actuators** placed in the same position of the sensors.

In order to avoid overconstraining the model, each spherical joint has been implemented with 3D linear springs, much stiffer (10^8 N/m) than the elastic elements of the system. This allows us to clearly identify the high frequency dummy resonances introduced in the transmissibility, and does not deteriorate the quality of the model.

8.2 HAM-SAS Model Linearization

The optical table is mounted on a two-stage suspension system, connected to the ground at a single point, as shown in Figure 8. This is the point at which the seismic excitation enters the system. To identify the transfer function between the input force and the optical table motion, the model needs to be disconnected from the ground. If the disconnection were total, the system could undergo rigid motion, which would create issues in generating a static equilibrium solution of the multibody model. To avoid this problem the system is actually connected to the ground by means of very soft dummy springs, which give eigenfrequencies well-separated from the lowest system frequencies, which are of the order of 0.1 Hz. The dummy springs are then removed from the state space model by using an output matrix C_e that extracts the motion of the excitation point. In fact, the force generated by the dummy springs of stiffness K is

$$\mathbf{u}_s = -\mathbf{K}z_e \quad (92)$$

$$= -\mathbf{K}C_e\mathbf{x}, \quad (93)$$

which results in a correction of the state-space representation of the system of the form

$$\mathbf{E}\dot{\mathbf{x}} = \mathbf{A}\mathbf{x} + \mathbf{B}(\mathbf{u} + \mathbf{u}_s) \quad (94)$$

$$= (\mathbf{A} - \mathbf{B}\mathbf{K}C_e)\mathbf{x} + \mathbf{B}\mathbf{u}. \quad (95)$$

Table 5: HAM-SAS modal analysis results.

Mode	Frequency (Hz)	
1	0.08001	table “pitch” mode
2	0.08841	table “roll” mode
3	0.10004	table vertical mode
4	0.27460	table “yaw” mode
5	0.34845	table horizontal mode
6	0.34845	table horizontal mode
7	2.29036	
8	2.29077	
9	2.77316	
10	32.82918	
11	32.82918	
12	32.82918	
13	32.82918	
14	32.82918	
15	32.83358	
16	32.83594	
17	32.83596	
18	58.48436	
19	65.61220	
20	109.41034	

The resulting eigenvalues are illustrated in Table 5, while the corresponding transfer function is illustrated in Fig. 9. The figure shows that all the displacements and the yaw rotation are allowed rigid body motion, while the pitch and roll motions saturate. This is a consequence of the fact that those motions involve an inverted pendulum device. Table 5 does not show that the free system contains four real, positive eigenvalues related to the inverted pendulum. This instability is purely theoretical, as the system is actually grounded, and in reality excitation occurs in terms of seismic (i.e. imposed) displacement of the ground point.

When the system has to be excited by imposing the motion of some part of it, a simple workaround uses the output matrix C_e that extracts the desired motion components z_e of the excitation point, and a co-located input matrix B_e that imposes the force components conjugated to z_e .

The desired motion components are thus the result of the problem

$$E\dot{x} = Ax + B_e u_e \quad (96)$$

$$z_e = C_e x \quad (97)$$

which, in the Laplace domain, can be written as

$$z_e = C_e (sE - A)^{-1} B_e u_e. \quad (98)$$

This problem must be invertible. The input required to impose the desired motion can thus be determined as

$$u_e = (C_e (sE - A)^{-1} B_e)^{-1} z_e, \quad (99)$$

so the regular system output is

$$z = C (sE - A)^{-1} B_e (C_e (sE - A)^{-1} B_e)^{-1} z_e. \quad (100)$$

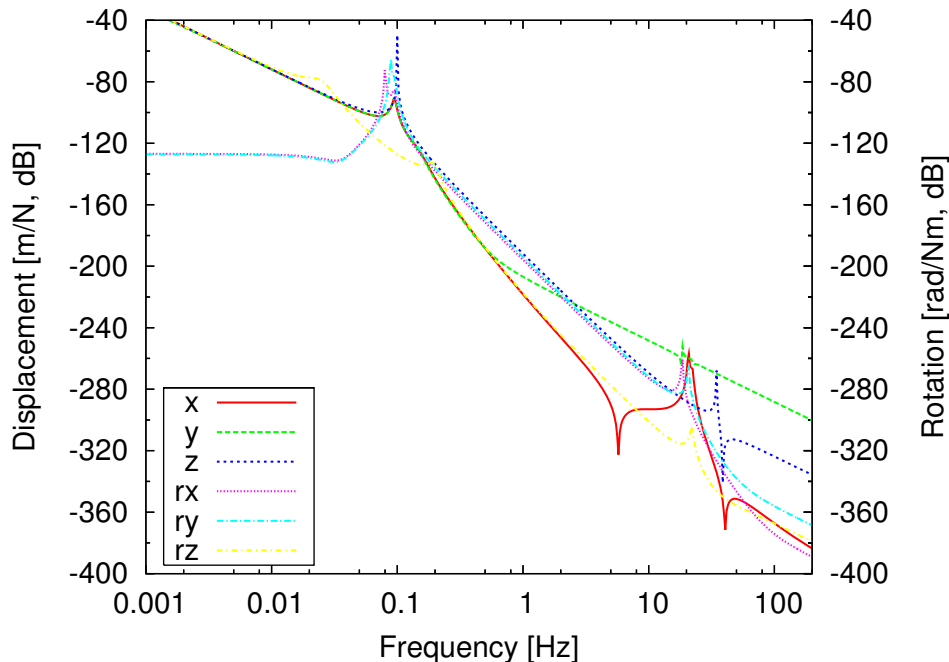


Figure 9: Dynamic response (displacements and rotations) of the HAM-SAS to excitation (forces and moments) at the connection to the ground.

The related transfer function is illustrated in Fig. 10.

Since the displacement that is used as excitation is located at the same point where the excitation forces are computed, the corresponding force-displacement transfer function must be exactly of order $1/s^2$, and its inversion does not represent a proper transfer function. However, when multiplied by the system's force-displacement transfer function, which is of order at least $1/s^2$, it will yield a proper displacement-displacement transfer function.

8.3 Experimental results

The installation and commissioning of HAM-SAS was done at the LASTI (LIGO Advanced System Test Interferometer) facility during a short period of less than four months. The LASTI is made up of standard full-scale LIGO vacuum chambers, arrayed in an 'L' configuration with arms lengths of 15 m. Measurements to characterize the performance of HAM-SAS mechanical system were done under vacuum to eliminate acoustic noise, air flow perturbations, and to reduce thermal drifts. Co-located sensing and actuation SISO and MIMO control strategy were successfully tested for DC control and damping low frequency resonances. We adopted a digital control system based on a real time Linux operating system with a sampling frequency of 2048 Hz, and 16-bit multichannel ADC and DAC PCI boards. We used voice-coil actuators with a geometry to minimize cross-coupling and noise injection, and LVDT displacement sensors with a typical resolution of $\sim 8\text{nm}/\sqrt{\text{Hz}}$ at 100 mHz, few-percent-level sensitivity to movements in other degrees of freedom and more than 10 mm of linear range. Some preliminary experimental results, such as transmissibilities and plant transfer functions, confirmed the validity of the direct model and its linearized synthesis.

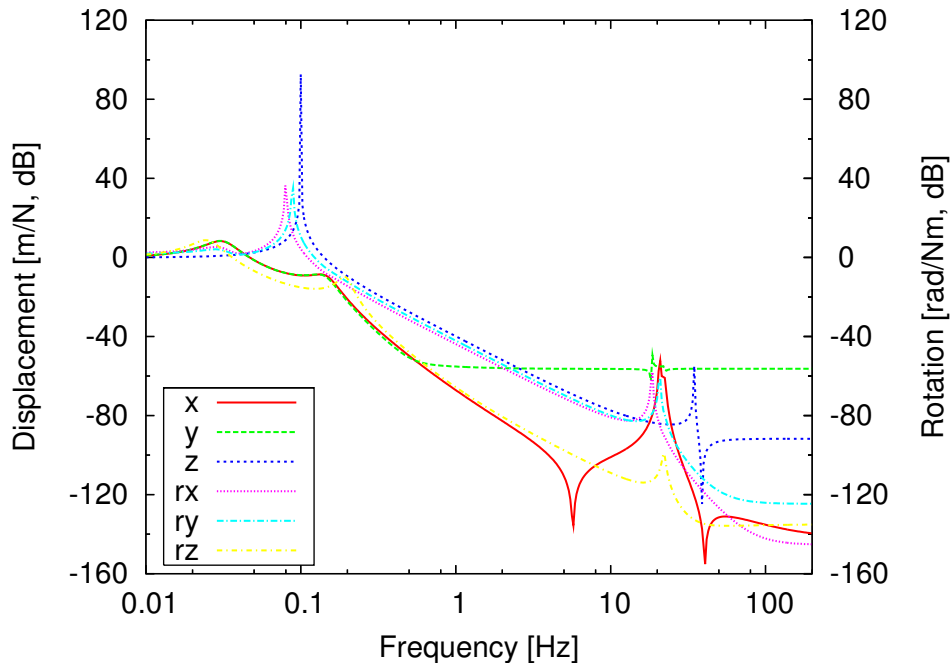


Figure 10: Dynamic response (displacements and rotations) of the HAM-SAS to excitation (displacements and rotations) at the connection to the ground.

8.3.1 Transmissibilities Measurements

The models were used to predict and then accurately describe the transmissibilities of the mechanical system. The transmissibility measurements were done using inertial velocity sensors. Six unidirectional geophones were placed on the optical table and suitably oriented to detect the residual excitation of all the six DOF. Similarly, three tri-axial force-feedback seismometers measured the six-DOF excitation of the ground. The ambient anthropogenic noise was used as excitation for the measurements.

Figure 11 shows the simulated and measured transmissibility along the horizontal Cartesian coordinate x from ground to the optical table. The first resonance at approximately 65 mHz corresponds to the IP flexible joints resonant frequency. The second peak at 125 mHz indicates a crosscoupling between the horizontal and vertical DOFs that is due to the fact that the Spring Box platform is probably tilted respect to ground. The third resonance at 265 mHz is caused by a horizontal resonant frequency of the MGAS springs. This resonance is due to the fact that the optical bench is connected to the MGAS filters by four vertical small piers. Those piers couple to the angular compliance of the MGAS filters, allowing horizontal motion. Below about 50 mHz the measurement showed almost zero coherence due to the poor sensitivity of the seismometers. Between 1 Hz and f , the measurement is mainly dominated by the geophone's electronic noise. Peaks between 15 Hz and 30 Hz are due to internal resonances attributed to the stabilizing device retrofitted to solve a pitch and roll instability caused by the high center of mass of the optical table's payload. Due to a lack of time, this device was made using simple helical springs and wires whose frequencies were too low. Replacing this temporary system with blades and stiffer structures and going through a thorough FEM design, such resonances should be moved higher in frequency, where the filtered seismic noise is negligible with respect to other noise sources in the interferometer.

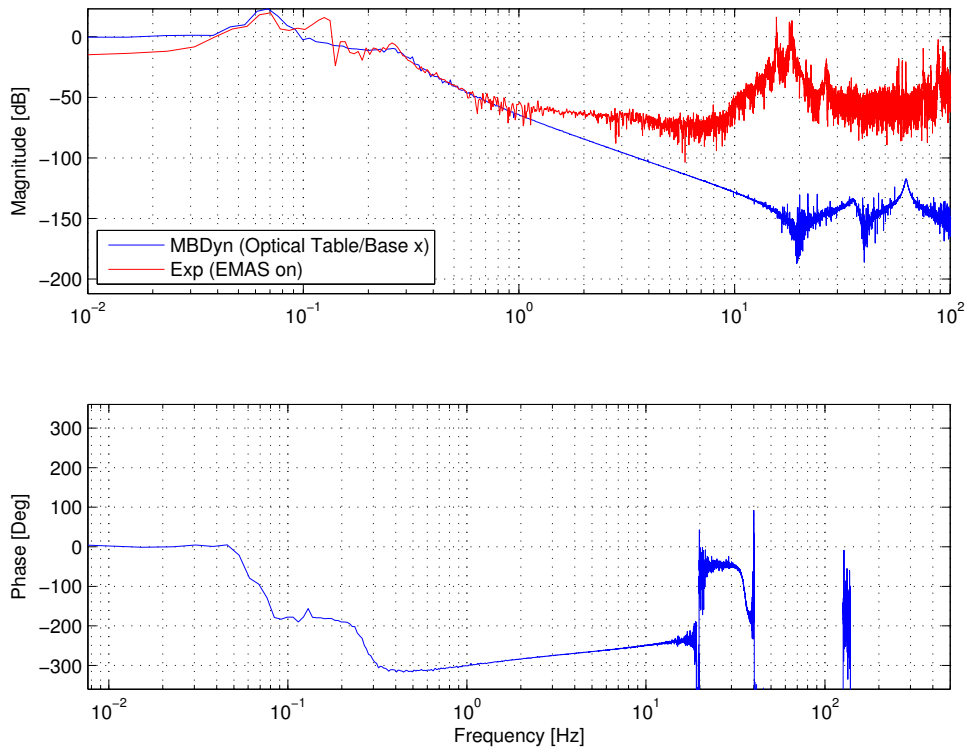


Figure 11: Comparison between the experimental transmissibility along direction x and the corresponding transmissibility obtained from the HAM-SAS MBDyn nonlinear model.

9 CONCLUSIONS

The work presented a technique to extract reduced order models, using normal modes, from the problem matrix generated by an existing free multibody software. The technique has been validated using simple analytical examples, and subsequently applied to a detailed model of the structural dynamics of the Horizontal Access Module Seismic Attenuation System (HAM-SAS) of the Laser Interferometer Gravitational wave Observatory (LIGO) experiment.

The reduced order model provides good fidelity with respect to small perturbation dynamics of the detailed multibody model, thus allowing us to efficiently synthesize the design of the HAM-SAS control system.

A key advantage is the possibility of obtaining the linearized model directly from the detailed nonlinear dynamics model used for time-domain analysis of the system, thus sharing the model development effort between the two phases.

10 ACKNOWLEDGMENTS

The LIGO Observatories were constructed by the California Institute of Technology and Massachusetts Institute of Technology with funding from the National Science Foundation under cooperative agreement PHY 9210038. The LIGO Laboratory operates under cooperative agreement PHY-0107417. This paper has been assigned LIGO Document Number LIGO-P070071-00-Z.

REFERENCES

- [1] A. Bertolini, R. DeSalvo, C. Galli, G. Gennaro, M. Mantovani, S. Márka, V. Sannibale, A. Takamori, and C. Torrie. Design and prototype tests of a seismic attenuation system for the advanced-LIGO output mode cleaner. *Classical and Quantum Gravity*, 23:S111–118, 2006.
- [2] A. Takamori, P. Raffai, S. Márka, R. DeSalvo, V. Sannibale, H. Tariq, A. Bertolini, G. Cella, N. Viboud, K. Numata, R. Takahashi, and M. Fukushima. Inverted pendulum as low frequency pre-isolation for advanced gravitational wave detectors. *submitted to Nuclear Instruments and Methods in Physics Research*.
- [3] G. Cella, V. Sannibale, R. DeSalvo, S. Márka, and A. Takamori. Monolithic geometric anti-spring blades. *Nuclear Instruments and Methods in Physics Research*, 540(2–3):502–519, 2005.
- [4] A. Stochino, R. DeSalvo, Y. Huang, and V. Sannibale. Improving the seismic noise attenuation performance of the monolithic geometric anti spring filters for gravitational wave interferometric detectors. *submitted to Nuclear Instruments and Methods in Physics Research*.
- [5] Pierangelo Masarati, Marco Morandini, Giuseppe Quaranta, and Paolo Mantegazza. Open-source multibody analysis software. In *Multibody Dynamics 2003, International Conference on Advances in Computational Multibody Dynamics*, Lisboa, Portugal, July 1–4 2003.
- [6] Giuseppe Quaranta, Pierangelo Masarati, and Paolo Mantegazza. Assessing the local stability of periodic motions for large multibody nonlinear systems using POD. *Journal of Sound and Vibration*, 271(3–5):1015–1038, 2004.
- [7] Gian Luca Ghiringhelli, Pierangelo Masarati, Paolo Mantegazza, and Mark W. Nixon. Multi-body analysis of a tiltrotor configuration. *Nonlinear Dynamics*, 19(4):333–357, August 1999.
- [8] John Denholm Lambert. *Numerical Methods for Ordinary Differential Systems*. John Wiley & Sons Ltd., Chichester, England, 1991.
- [9] Kathryn Eleda Brenan, Stephen La Vern Campbell, and Linda R. Petzold. *Numerical Solution of Initial-Value Problems in Differential-Algebraic Equations*. North-Holland, New York, 1989.
- [10] Gian Luca Ghiringhelli, Pierangelo Masarati, and Paolo Mantegazza. A multi-body implementation of finite volume beams. *AIAA Journal*, 38(1):131–138, January 2000.